



ISSN NO. 2320-5407

Journal homepage: <http://www.journalijar.com>

INTERNATIONAL JOURNAL
OF ADVANCED RESEARCH

RESEARCH ARTICLE

CAUSE AND CATASTROPHE OF STRENGTHENING MECHANISMS IN 7020/AL₂O₃ COMPOSITES PREPARED BY STIR CASTING PROCESS AND VALIDATION THROUGH FEA

A. Chennakesava Reddy

Professor, Department of Mechanical Engineering, JNTUH College of Engineering Kukatpally, Hyderabad – 500 085, Telangana, India.

Manuscript Info

Manuscript History:

Received: 12 January 2015
Final Accepted: 23 February 2015
Published Online: March 2015

Key words:

7020, alumina, Metal matrix composites (MMCs), strength, analytical modelling, mechanical testing.

*Corresponding Author

A. Chennakesava Reddy

Abstract

The present research has been focused to study causes and misfortunes of strengthening mechanisms in 7020/Al₂O₃ metal matrix composites. It was found that the tensile strength and stiffness increase with increasing volume fraction of Al₂O₃ particulates. The tensile strength and stiffness were decreased with increased size of particulates. After heat treatment, most of the coarse intermetallic phases are dissolved to form stable MgZn₂, Al₂Mg₃Zn₃, and Al₂CuMg compounds. A clustering of particulates was observed in the composites having very small particles. The wettability and uniform distribution of particles have improved the strengthening mechanism. The proposed formulae by the author for the tensile strength and elastic modulus could predict them very close to the experimental values of 7020/Al₂O₃ composites. The FEA results validate the occurrence of particle debonding, porosity, and clustering in the composites.

Copy Right, IJAR, 2015., All rights reserved

INTRODUCTION

The 7020 aluminium alloy is used as cladding material on the coolant side of heat exchanger components. The 7020 alloy is used as structural armor alloy. Performance measures of the structural armors include low cost and capabilities for ballistic and blast protection, weld fabricability, and durability against stress corrosion cracking and exfoliation corrosion. Reinforcement by particulates of Al₂O₃ has proved to be exclusively beneficial as it offers the metal matrix composites at low price. In spite of their exceptional mechanical properties, Al-Al₂O₃ composites fabricated through casting route, suffer disadvantageous effects such as sedimentation of particulates, higher porosity level, poor wettability, clustering and cracking of particulates and interfacial reactions (Rohatgi et al., 1986; Reddy, 2009; Reddy and Essa, 2010). Redsten et al. (1995) have investigated the influence of 25 vol. %, 0.28µm Al₂O₃ particles dispersed in Al. They found that the 0.2% proof stress and ultimate tensile strength were found to be about 200 MPa and 330 MPa respectively. Srivatsan (1996) has studied the fracture behaviour of 2011 Al alloy reinforced with two different volume fractions of 10 and 15% Al₂O₃. The tensile strength in the 15 vol. % composite was found to be 2% more than that of the 10 vol. % composite. The tensile fracture surface shows brittle appearance on macroscopic scale and microscopically local ductile and brittle fracture. Kamat et al. (1989) have performed different tests on 2011-O and 2024-O Al alloy reinforced with Al₂O₃ having 2 to 20 % volume fraction with different particle sizes. They found that the yield strength was increased with decrease in spacing between particles. Pestes et al. (1994) have studied the effect of particle size on the fracture toughness of Al/Al₂O₃ composites. They

established that an increase in the inter-particle spacing could increase the toughness either by decreasing the volume fraction of particulates or increasing size of the particles.

All these phenomena may influence the tensile strength and stiffness of composite. With this underlying background, the motivation for this article is to study the influence of volume fraction and particle size of Al_2O_3 reinforcement, clustering of particles, the formation of precipitates at the particle / matrix interface, cracking of particles, and voids/porosity on the elastic modulus and tensile strengths of 7020/ Al_2O_3 metal matrix composites.

2. ANALYTICAL MODELS

For a tensile testing of a rectangular cross-section, the tensile strength is given by:

$$\sigma_t = \frac{F_t}{A_t} \quad (1)$$

The engineering strain is given by:

$$\varepsilon_t = \frac{\Delta L_t}{L_{t0}} = \frac{L_t - L_{t0}}{L_{t0}} \quad (2)$$

where ΔL_t is the change in gauge length, L_0 is the initial gauge length, and L_t is the final length, F_t is the tensile force and A_t is the nominal cross-section of the specimen.

The Weibull cumulative distribution can be transformed so that it appears in the familiar form of a straight line:

$Y = mx + b$ as follows:

$$F(x) = 1 - e^{-\left(\frac{x}{\alpha}\right)^\beta} \quad (3)$$

$$\ln\left[\ln\left(\frac{1}{1-F(x)}\right)\right] = \beta \ln x - \beta \ln \alpha \quad (4)$$

Comparing this equation with the simple equation for a line, we see that the left side of the equation corresponds to Y , $\ln x$ corresponds to X , β corresponds to m , and $-\beta \ln \alpha$ corresponds to b . Thus, when we perform the linear regression, the estimate of the Weibull parameter (β) comes directly from the slope of the line. The estimate of the parameter (α) must be calculated as follows:

$$\alpha = e^{-\left(\frac{b}{\beta}\right)} \quad (5)$$

According to the Weibull statistical-strength theory for brittle materials, the probability of survival, P at a maximum stress (σ) for uniaxial stress field in a homogeneous material governed by a volumetric flaw distribution is given by

$$P(\sigma_f \geq \sigma) = R(\sigma) = e^{-B(\sigma)} \quad (6)$$

where σ_f is the value of maximum stress of failure, R is the reliability, and β is the risk of rupture. A non-uniform stress field (σ) can always be written in terms of the maximum stress as follows:

$$\sigma(x, y, z) = \sigma_{0f}(x, y, z) \quad (7)$$

For a two-parameter Weibull model, the risk of rupture is of the form

$$B(s) = A \left(\frac{\sigma}{\sigma_0}\right)^\beta \quad (\sigma_0, \beta > 0) \quad (8)$$

where $A = \int_v [f(x, y, z)]^\beta dv$ (9)

and σ_0 is the characteristic strength, and β is the shape factor that characterizes the flaw distribution in the material. Both of these parameters are considered to be material properties independent of size. Therefore, the risk to break will be a function of the stress distribution in the test specimen. Equation (8) can also be written as

$$B(\sigma) = \left(\frac{\sigma}{\sigma_A}\right)^\beta \quad (10)$$

$$\sigma_A = \sigma [A]^{-\frac{1}{\beta}} \quad (11)$$

And the reliability function, Eq. (11) can be written as a two-parameter Weibull distribution

$$R(\sigma) = e - \left(\frac{\sigma}{\sigma_A} \right)^\beta \quad (12)$$

The tensile tests of specimens containing different stress fields can be represented by a two-parameter Weibull distribution with the shape parameter and characteristic strength. The authors have proposed expression for the tensile strength considering the effects of reinforced particle size and voids/porosity. The expression of tensile strength is given below:

$$\sigma_t = \sigma_0 [V_m + V_p - V_v]^{-1/\beta} \quad (\sigma_0, \beta_t > 0) \quad (13)$$

where σ_0 is the characteristic strength of tensile loading, β is the shape parameter which characterize the flaw distribution in the tensile specimen, V_m , V_p , and V_v are respectively volume of the matrix, volume of the reinforced particles and volume of the voids/porosity in the tensile specimen.

3. EXPERIMENTAL PROCEDURE

The composites were prepared by the stir casting and low-pressure die casting process. The matrix alloy was 7020. The reinforcement was Al_2O_3 particulates. The volume fractions of Al_2O_3 reinforcement are 12%, 16%, and 20%. The particle sizes of Al_2O_3 reinforcement are 2 μm , 5 μm , and 10 μm .

3.1 Preparation of Melt and Metal Matrix Composites

The 7020 matrix alloy was melted in a resistance furnace. The crucibles were made of graphite. The melting losses of the alloy constituents were taken into account while preparing the charge. The charge was fluxed with coverall to prevent dressing. The molten alloy was degasified by tetrachlorethane (in solid form). The crucible was taken away from the furnace and treated with sodium modifier. Then the liquid melt was allowed to cool down just below the liquidus temperature to get the melt semi solid state. At this stage, the preheated (500 $^\circ\text{C}$ for 1 hour) reinforcement particles were added to the liquid melt. The molten alloy and reinforcement particles are thoroughly stirred manually for 15 minutes. After manual steering, the semi-solid, liquid melt was reheated, to a full liquid state in the resistance furnace followed by an automatic mechanical stirring using a mixer to make the melt homogenous for about 10 minutes at 200 rpm. The temperature of melted metal was measured using a dip type thermocouple. The preheated cast iron die was filled with dross-removed melt by the compressed (3.0 bar) argon gas (Reddy, 2009; Reddy, 2010).

3.2 Heat Treatment

Prior to the machining of composite samples, a solution treatment was applied at 600 $^\circ\text{C}$ for 1 hour, followed by quenching in cold water. The samples were then naturally aged at room temperature for 100 hours.

3.3 Tensile Tests

The heat-treated samples were machined to get flat-rectangular specimens (figure 1) for the tensile tests. The tensile specimens were placed in the grips of a Universal Test Machine (UTM) at a specified grip separation and pulled until failure. The test speed was 2 mm/min (as for ASTM D3039). A strain gauge was used to determine elongation.

3.4 Optical and Scanning Electron Microscopic Analysis

An image analyser was used to study the distribution of the reinforcement particles within the 7020 aluminium alloy matrix. The polished specimens were ringed with distilled water, and etched with 0.5% HF solution for optical microscopic analysis. Fracture surfaces of the deformed/fractured test samples were analysed with a scanning electron microscope (SEM) to define the macroscopic fracture mode and to establish the microscopic mechanisms governing fracture. Samples for SEM observation were obtained from the tested specimens by sectioning parallel to the fracture surface and the scanning was carried using S-3000N Toshiba SEM.

3.5 Finite Element Analysis

Particle distribution, clustering and porosity in the composite were modelled using ANSYS software (Chennakesava, 2008). A test coupon of 0.03mm x 0.03mm composite was modelled to examine particle clustering, debonding. In addition, a porosity of 36 μm was modelled in the test coupon of 0.1mm x 0.1mm. A triangle element of 6 degrees of freedom was used to mesh the Al_2O_3 particle, precipitates and the matrix alloy. For load transfer from the matrix to the particle point-to-point coupling of zero length was used. The test coupon was tensile loaded. Assuming that the metal matrix is linear leads to the following system of discrete equations:

$$\begin{bmatrix} k^{00} & \dots & k^{06} \\ \vdots & \ddots & \vdots \\ k^{16} & \dots & k^{66} \end{bmatrix} \begin{bmatrix} d^2 \\ \vdots \\ d^6 \end{bmatrix} = \begin{bmatrix} Q^2 \\ \vdots \\ Q^6 \end{bmatrix} \quad (14)$$

where $d^i = [d^0 \dots d^6]^T$ is the finite element degrees of freedom, $Q^i = [Q^0 \dots Q^6]^T$ is the load vector and k^{ii} stiffness coefficient.

The dislocation loop is represented by two levels sets $f(x)$ and $g(x)$. The dislocation line is the intersection of $f(x) = 0$ and $g(x) = 0$. The presence of dislocation line is $\zeta = \Lambda f \times \Lambda g$. The discrete equations for dislocations are given by

$$K^{uu} d^u = f^{ext} - \sum_{i=0}^1 K^{ui} q^i \quad (15)$$

The stiffness matrix is independent of the number, orientation and location of the dislocations. In addition, since the effect of the dislocation appears only as a nodal force, the dislocation model is easily incorporated into ANSYS. In the present work the element edges were aligned with the grain boundaries and phase interfaces. The interface was assumed to be $MgZn_2$ at grain boundaries. The crack propagation was not considered for the finite element modelling, however the likelihood of particle or matrix cracking was identified by the stress that exceeds the allowable stress of alumina particle or 7020 matrix alloy.

4. RESULTS AND DISCUSSION

The modulus of elasticity is the stiffness of the composite. The modulus of elasticity is improved by the addition of Al_2O_3 particles. The composites can fail on the microscopic or macroscopic scale. The tensile strength is the maximum stress that the material can sustain under a uniaxial loading. For metal matrix composites, the tensile strength depends on the scale of stress transfer from the matrix to the particulates.

4.1 Cause of Strengthening Mechanisms

The variation of tensile strength with volume fraction and particle size is shown in figure 2. It is clearly shown that, for a given particle size the tensile strength increases with an increase in the volume fraction of Al_2O_3 . As the particle size decreases the tensile strength increases. This is due to fact that the smaller particles have a larger surface area for transferring stress from the matrix. The other possibility, of increasing strength is owing to the formation of precipitates at the particle/matrix interface. The microstructure of heat treated composite is shown in figure 3a. It is observed that the microstructure consists of equilibrium phases of $Al + MgZn_2$, $Al + MgZn_2 + AlCuMg$ and Al_2O_3 particulates. The weight percentages of different phases formed in the composite are shown in figure 3b. The 7020 alloy undergoes phase dissolution at $325^\circ C$. It emerges that the $Al + MgZn_2 + Al_2Mg_3Zn_3$ phases diminish, and the $Al + MgZn_2$ and $Al + Al_2Mg_3Zn_3 + AlCuMg$ phases become more significant. The $MgZn_2$ precipitates tend to dissolve above $325^\circ C$ and then harden by natural aging at room temperature to achieve mechanical properties of high tensile strength and strain hardening. As the melt was treated with Mg to improve wettability, the chemistry of 7020/ Al_2O_3 composite appears to reach a most favorable Mg content for strengthening while retaining low contents of Mg + Zn. During solidification of 7020/ Al_2O_3 composites, the predominant phase formed during solidification is Al_6Mn . The objective of solution treatment is to breakdown, or partial breakdown of $Al_6(FeMn)$ or Al_6Mn intermetallic phase, to alpha ($AlFeMnSi$). There is competition between and Mg_2Si as the temperature is lowered and Mg_2Si is formed over preference to, lowering the amount of α . 7020/ Al_2O_3 composites achieve maximum strain hardening due to precipitation of the metastable phases related to stable counterparts of $MgZn_2$, $Al_2Mg_3Zn_3$, and Al_2CuMg . The precipitation hardening also influences the direct strengthening of the composite due to heat treatment. An increase in volume fraction with smaller particles of Al_2O_3 increases the amount of strengthening owing to increasing obstacles to the dislocations. This is because, smaller particle size means a lower inter-particle spacing so that nucleated voids in the matrix are unable to coalesce as easily.

Finite element model of test coupon of size $0.03mm \times 0.03mm$ consisting of uniformly distributed particles of $10\mu m$ size is shown figure 4a. The volume fraction of Al_2O_3 is nearly 21%. The maximum tensile strength is 315.664 MPa (figure 4b) whereas the experimental value is 302.715 MPa. This is error is due to assumption of uniform distribution of particles in the matrix. The maximum stress-intensity values are found over the particles (figure 4c) and in the regions between the particles where the debonding (C) occurs as shown in figure 5. There is accumulation of dislocations in the path from the matrix to the particles through the matrix/particle interface collinear to the direction of tensile loading as shown in figure 4d. The stress intensity peaks across the centre line particles in the direction of tensile loading is shown in figure 4e. The stress intensity is highly concentrated at the

particle cites. The same kind of phenomena is observed with strain-intensity values (figure 5f) at the particle/matrix interface. The Al_2O_3 particle experiences low level of strains as compared to the matrix because of their stiffness value of 476 GPa (figure 4f). The deformation of particles is negligible as compared to the matrix. This gives an impression of near uniform distribution of particles in the matrix due to two-level mechanical stirring and addition of Mg as a wetting agent.

4.2 Catastrophe of strengthening mechanisms

As the particle size increases the tensile strength decreases as shown in figure 2. The coarser particles were more likely to contain flaws, which might severely reduce their strength than smaller particles. There is a possibility of clustering (A) of Al_2O_3 particles as seen in figure 5. These clusters act as sites of stress concentration. At higher volume fractions the particle-particle interaction may develop clustering in the composite. The formation of clustering increases with an increase in the volume fraction and with a decrease in the particle size. A five-particle clustering (particle size = $2\mu m$ and volume fraction = 20%) is modeled in ANSYS as shown in figure 6a. The experimental tensile strength is 360.80 MPa. The FEA result is 343.896 MPa (figure 6b). The transfer of load from the matrix to the particle via the matrix/particle interface and vice-versa is seen in figure 6c. The density of dislocations is highly colonized due to obstruction of the particle around it. The reduction of strength is due to debonding (C in figure 5) of particles in the direction of tensile loading. The maximum strain intensity is also observed at the clustering interface of particles as seen in figure 6d, but the strain intensity in the particle is less (figure 6e).

Non-planar cracking (D) of particle (figure 5) was observed in the 7020/ Al_2O_3 composite comprising $10\mu m$ particles. This is because of the low passion's ratio (0.21) of Al_2O_3 particle as than that (0.33) of the matrix alloy. There is every possibility of cavity formation during the preparation of composite or during testing of composite due to debonding (C) as shown in figure 5. The porosity (B as shown in figure 5) of approximately $36\mu m$ is also revealed in the 7020/ Al_2O_3 composite having $10\mu m$ particles. Finite element model of test coupon of size $0.1mm \times 0.1mm$ consisting of particles of size of $10\mu m$ is shown figure 7a. The loss of strength due to porosity is nearly 19.716 MPa. The distribution of stress vectors around the cavity is shown in figure 7b. The maximum stress intensities are found in the matrix along the transverse direction of tensile loading as shown in figure 7c. The interruption of stress intensity curve (figure 7d) is on account of porosity present in the composite.

4.3 Strengthening Mechanisms

The strength of a particulate metal matrix composite depends on the strength of the weakest zone and metallurgical phenomena in it. Even if numerous theories of composite strength have been published, none is universally taken over however. Along the path to the new criteria, we attempt to understand them.

For very strong particle-matrix interfacial bonding, Pukanszky et al. (1988) presented an empirical relationship as given below:

$$\sigma_c = \left[\sigma_m \left(\frac{1 - v_p}{1 + 2.5v_p} \right) \right] e^{Bv_p} \quad (16)$$

where B is an empirical constant, which depends on the surface area of particles, particle density and interfacial bonding energy. The value of B varies between from 3.49 to 3.87. The strength values obtained from this criterion are approaching the experimental values of the composites as shown in figure 8a. This criterion has taken care of the presence of particulates in the composite and interfacial bonding between the particle/matrix. The effect of particle size and voids/porosity were not considered in this criterion.

Hojo et al. (1974) found that the strength of silica-filled epoxy decreased with increasing mean particle size d_p according to the relation

$$\sigma_c = \sigma_m + k(v_p)d_p^{-1/2} \quad (17)$$

where $k(v_p)$ is a constant being a function of the particle loading. This criterion holds good for small particle size, but fails for larger particles as shown in figure 8b. Withal, the composite strength decreases with increasing filler-loading in the composite.

A new criterion is suggested by the author considering adhesion, formation of precipitates, particle size, agglomeration, voids/porosity, obstacles to the dislocation, and the interfacial reaction of the particle/matrix. The formula for the strength of composite is stated below:

$$\sigma_c = \left[\sigma_m \left(\frac{1 - (v_p + v_v)^{2/3}}{1 - 2(v_p + v_v)} \right) \right] e^{m_m(v_p + v_v)} + k(v_p) m_p d_p^{-1/2} \quad (18)$$

where v_v is the volume fraction of voids/porosity in the composite, m_m and m_p are the poisson's ratios of the matrix and particulates, and $k(v_p)$ is the slope of the tensile strength against the mean particle size (diameter) and is a function of particle volume fraction v_p . The predicted strength values are within the allowable bounds of experimental strength values as shown in figure 8c.

4.4 Elastic Modulus

Elastic modulus (Young's modulus) is a measure of the stiffness of a material and is a quantity used to characterize materials. Elastic modulus is the same in all orientations for isotropic materials. Anisotropy can be seen in many composites. Alumina (Al_2O_3) has much higher Young's modulus (is much stiffer) than 7020 aluminium alloy.

Ishai and Cohen (1967) developed based on a uniform stress applied at the boundary, the Young's modulus is given by

$$\frac{E_c}{E_m} = 1 + \frac{1 + (\delta - 1)v_p^{2/3}}{1 + (\delta - 1)(v_p^{2/3} - v_p)} \quad (19)$$

which is upper-bound equation. They assumed that the particle and matrix are in a state of macroscopically homogeneous and adhesion is perfect at the interface. The lower-bound equation is given by

$$\frac{E_c}{E_m} = 1 + \frac{v_p}{\delta / (\delta - 1) - v_p^{1/3}} \quad (20)$$

where $\delta = E_p / E_m$.

The proposed equation by the author to find Young's modulus includes the effect of voids/porosity in the composite as given below:

$$\frac{E_c}{E_m} = \left(\frac{1 - v_v^{2/3}}{1 - v_v^{2/3} + v_v} \right) + \left(\frac{1 + (\delta - 1)v_p^{2/3}}{1 + (\delta - 1)(v_p^{2/3} - v_p)} \right) \quad (21)$$

The results of Young's modulus derived from the proposed equation (21) are approximately equal to the experimental values and these values are also matching with those computed by Ishai and Cohen criteria (table 1).

4.5 Weibull Statistical Strength Criterion

The tensile strength of 7020/ Al_2O_3 was analysed by Weibull statistical strength criterion using Microsoft Excel software. The slope of the line, β , is particularly significant and may provide a clue to the physics of the failure. The Weibull graphs of tensile strength indicate lesser reliability for filler loading of 12% than those reliabilities of 16, and 20 (figure 9a). The shape parameters, β s (gradients of graphs) are 12.190, 16.376 and 17.403 respectively, for the composites having the particle volume fraction of 12%, 16%, and 20%.

The Weibull characteristic strength is a measure of the scale in the distribution of data. It so happens that 63.2 percent of the composite has failed at σ_0 . In other words, for a Weibull distribution $R (=0.368)$, regardless of the value of β . With 7020/ Al_2O_3 , about 36.8 percent of the tensile specimens should survive at least 285.289 MPa, 328.061 MPa, and 348.749 MPa for 12%, 16%, and 20% volume fractions of Al_2O_3 in the specimens respectively. The reliability graphs of tensile strength are shown in figure 9b. At reliability 0.90 the survival tensile strength of 7020/ Al_2O_3 containing 12% of volume fraction is 237.196 MPa, 16% of volume fraction is 285.940 MPa, and 20% of volume fraction is 306.446 MPa. This clearly indicates that the tensile strength increases with increase in volume fraction of Al_2O_3 . These results are matching with those of FEA results with an error ranging 2.69 to 4.14%.

4.5 Fracture

Fractography (figure 10) reveals microscopically local ductile and brittle mechanisms. Failure of the composite was found to occur by particle cracking and particle-matrix decohesion at the interface. The fracture process in a high

volume fraction (20%) aluminium/ Al_2O_3 composite is very much localized. The failure path in these composites is from the matrix to the particle through the matrix/particle interface elongation or cracking as stated by Chennakesava Reddy (2002). The presence of Al_2O_3 reinforcement particles reduces the average distance in the composite by providing strong barriers to dislocation motion. The interaction of dislocations with other dislocations, precipitates, and Al_2O_3 particles causes local accumulation of the dislocations. The presence of voids is also observed in the composites having larger Al_2O_3 particles. The void coalescence occurs when the void elongates to the initial intervvoid spacing.

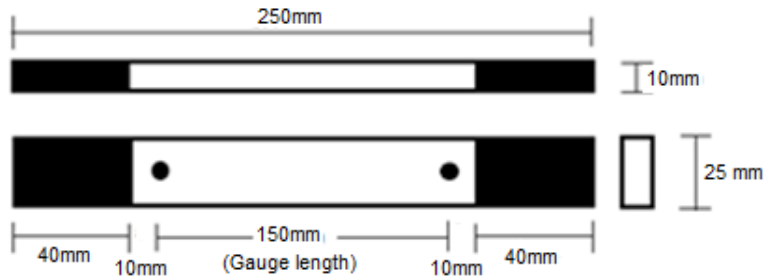


Figure 1: Shape and dimensions of tensile specimen

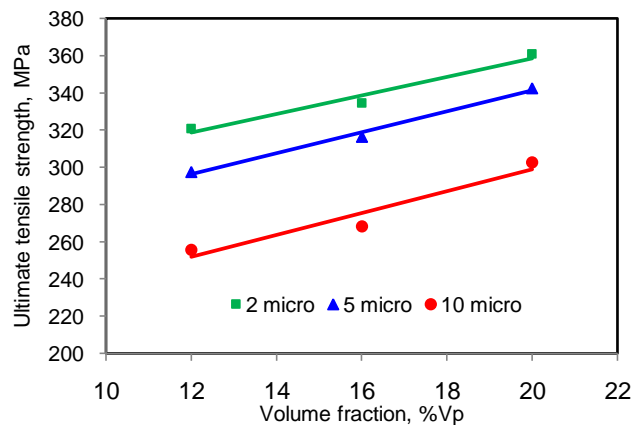


Figure 2: Variation of the tensile strength with the volume fraction and particle size of Al_2O_3

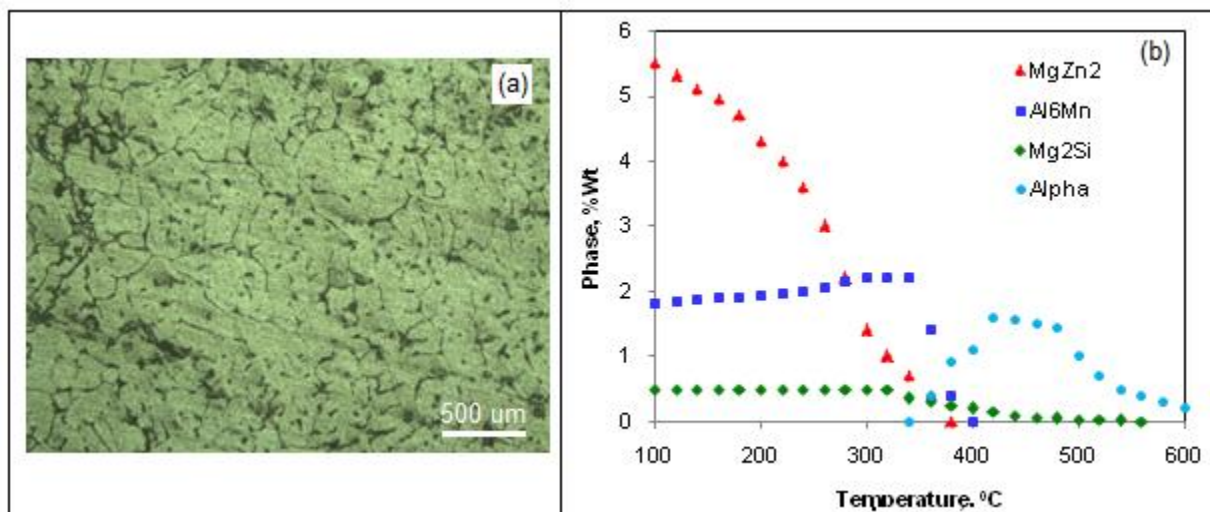


Figure 3: Microstructure of heat treated composite (a), Precipitates in the composite (b), (Al_2O_3 particle size = $10\mu\text{m}$ and $V_p = 20\%$).

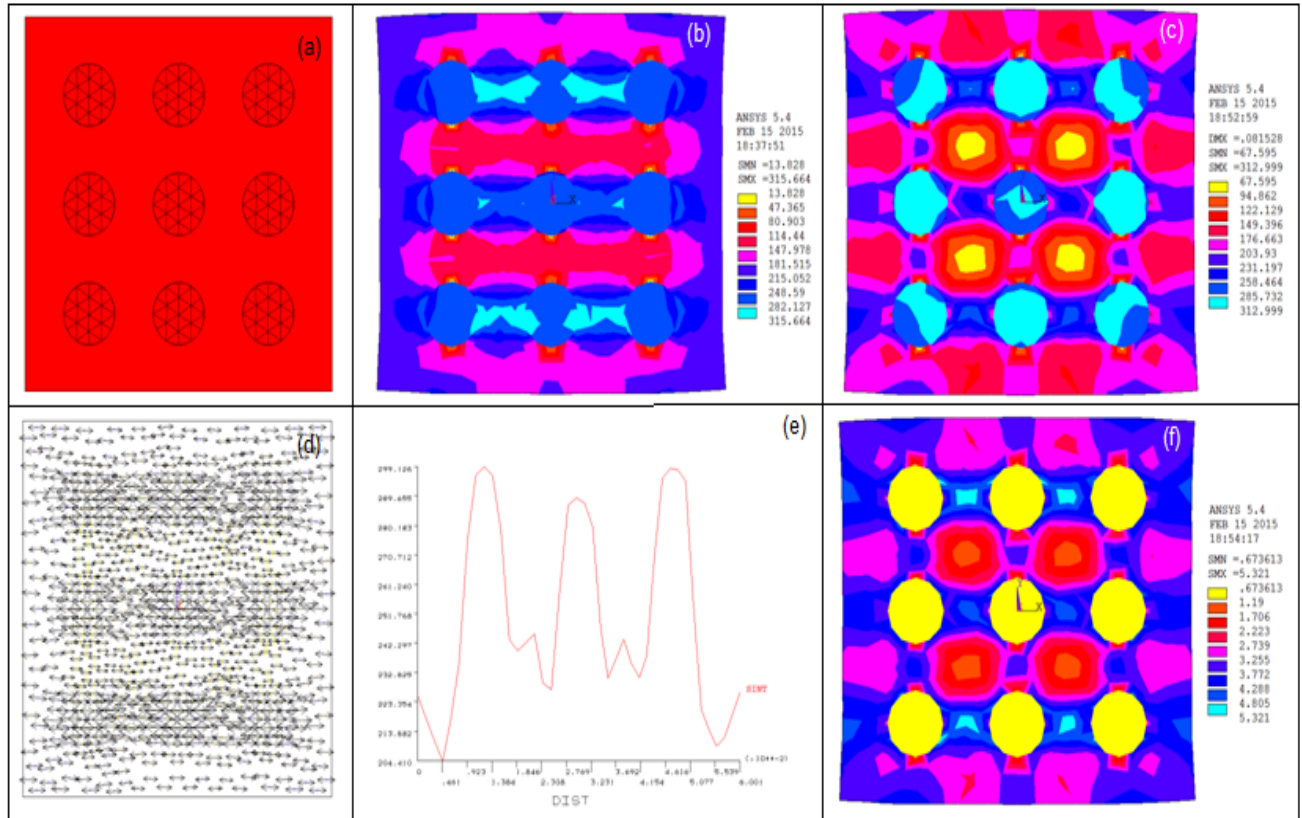


Figure 4: Particle distribution (a), Stress variation in the load direction (b), Stress intensity variation (c), stress vector flow (d), stress variation along centre line in the load direction (e), and strain intensity variation (f).

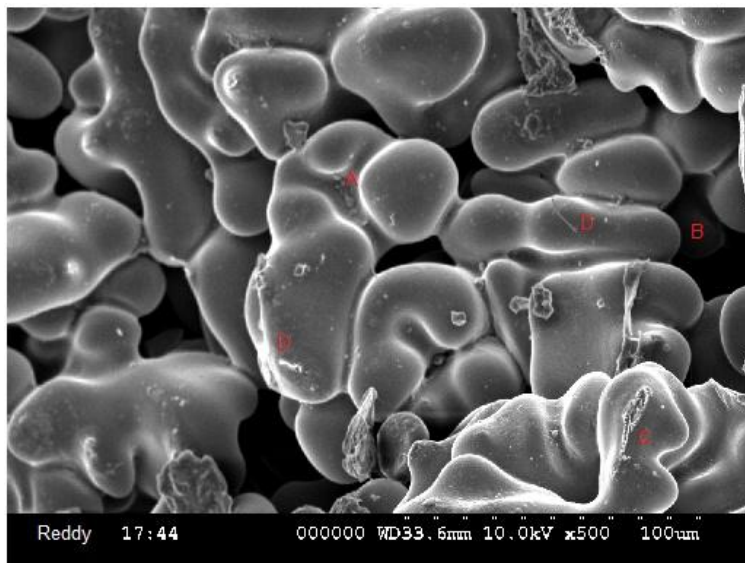


Figure 5: Particle clustering, particle cracking, debonding and porosity

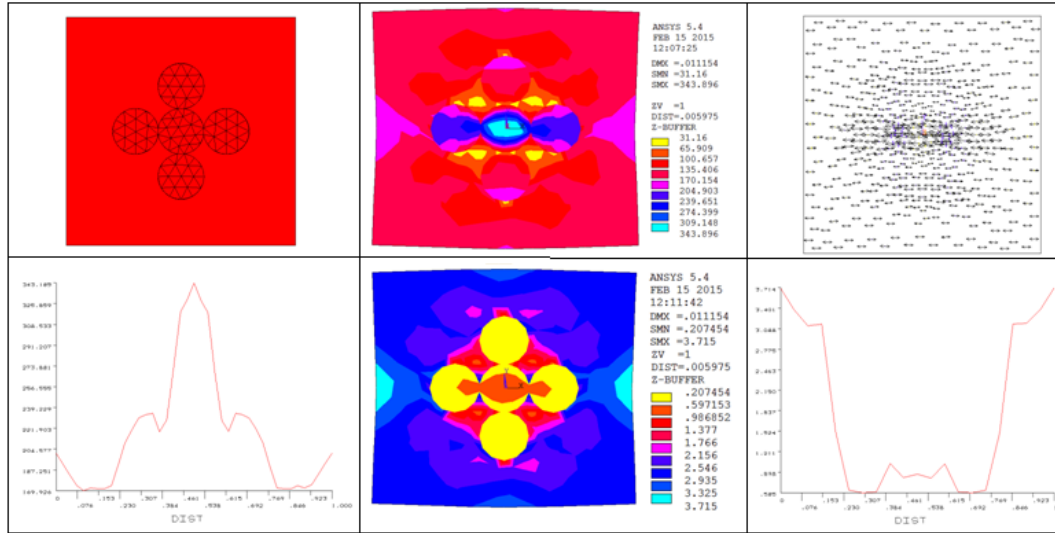


Figure 6: Particle clustering (a), stress variation in the load direction (b), stress vector flow (c), stress intensity variation (d), strain intensity (e), and strain intensity variation along the centre line in the load direction (f).

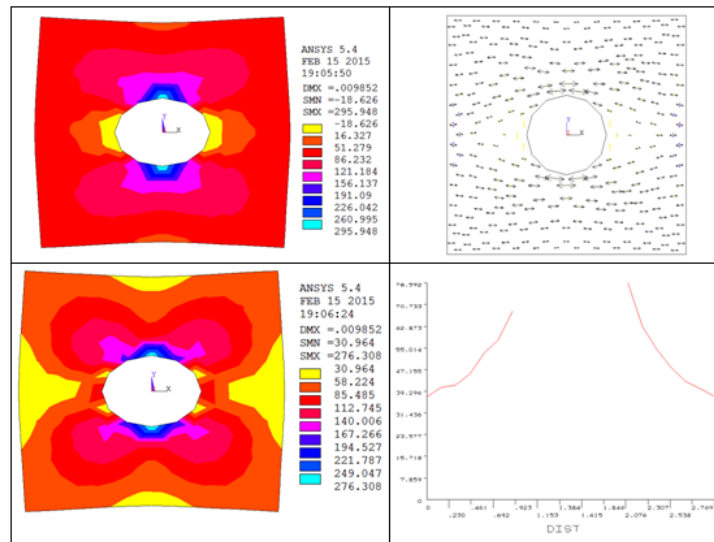


Figure 7: stress variation in the load direction due to Porosity (a), stress vector flow (b), stress intensity variation (c), and strain intensity variation along the centre line in the load direction (d).

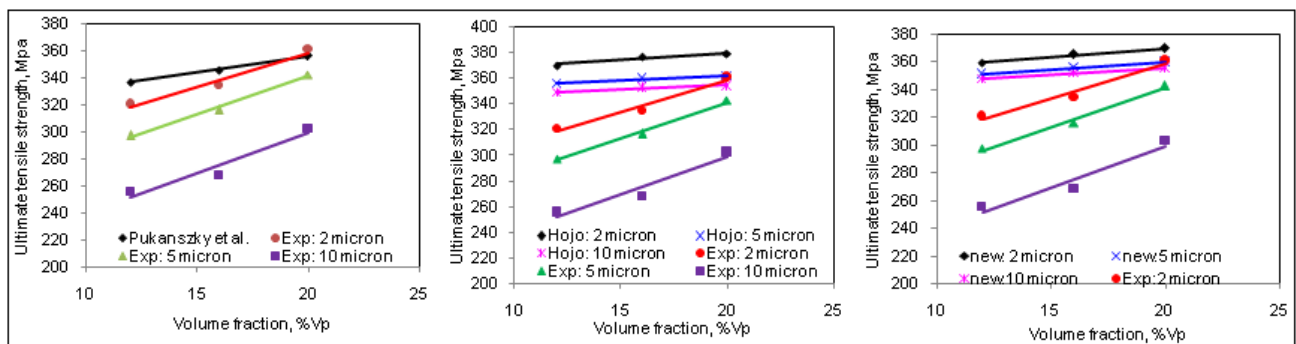


Figure 8: Comparison of calculated experimental tensile strength values with Pukanszky et al criterion (a), Hojo criterion (b), and proposed criterion (c).

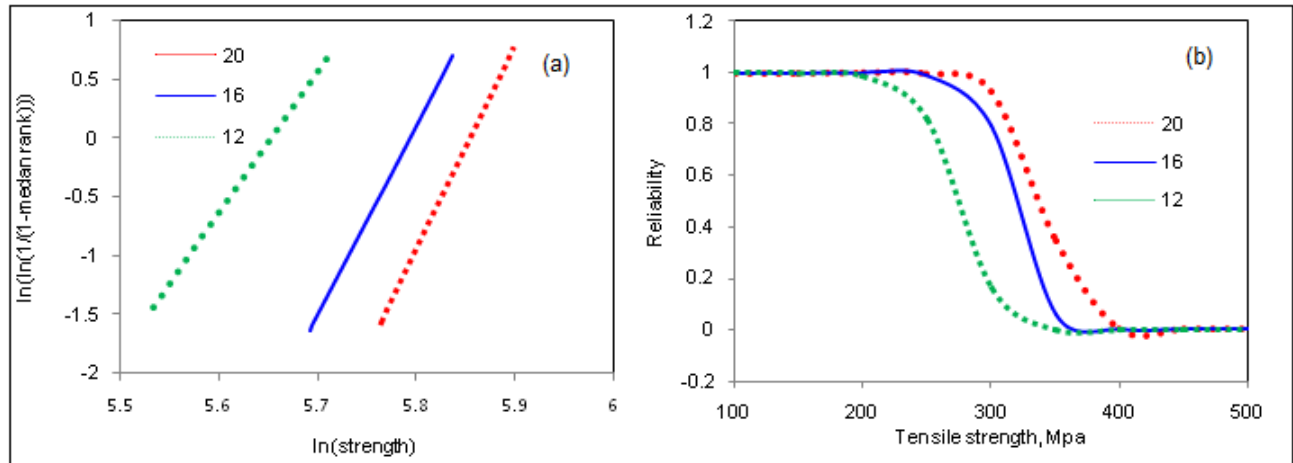


Figure 9: Weibull distribution of tensile strength (a), and Reliability graphs for tensile strength (b).

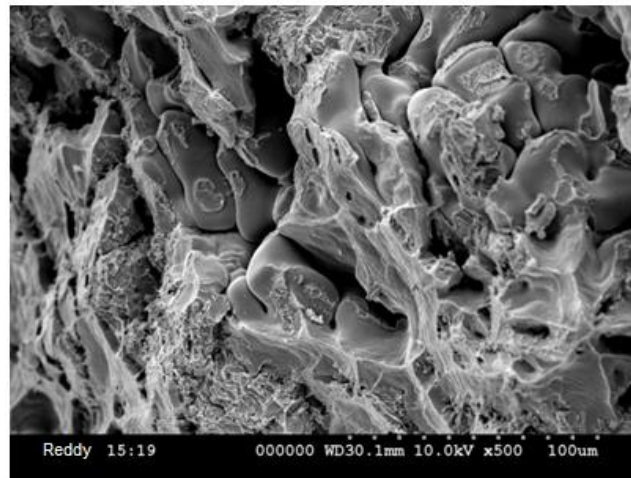


Figure 10: SEM of fracture surface of composite (20% Vf and 10 μm particle size of Al₂O₃ in 7020).

Table 1: Young’s modulus obtained from various criteria

Criteria	Young’s modulus, GPa		
	V _p =12	V _p =16	V _p =20
Ishai and Cohen (upper bound)	172.87	181.03	189.19
New proposal from Author	171.61	179.51	186.95

5. CONCLUSIONS

The stable precipitates such as MgZn₂, Al₂Mg₃Zn₃, and Al₂CuMg were observed in the 7020/Al₂O₃ composites. The porosity of approximately 36μm was also revealed in the 7020/Al₂O₃ composite having 10μm particles. At higher volume fractions concentration, i.e., small interparticle distances, the particle-particle interaction may develop agglomeration in the composite. Non-planar cracking of particle was observed in the 7020/Al₂O₃ composite comprising 10μm particles. The tensile strength increases with increase in volume fraction of Al₂O₃, whereas it decreases with increasing particle size. The experimental values of tensile strength and Young’s modulus are nearly equal to the predicted values by the new formulae proposed by the author. The FEA results confirm the occurrence of particle debonding, porosity, and clustering in the composites.

ACKNOWLEDGEMENTS

The author acknowledges with thanks University Grants Commission (UGC) – New Delhi for sectioning R&D project, and Tapasya Casting Private Limited – Hyderabad, and Indian Institute of Chemical Technology- Hyderabad for their technical help.

REFERENCES

- Chennakesava R. Alavala. (2002): Fracture behavior of brittle matrix and alumina trihydrate particulate composites, *Indian Eng. Mat. Sci.*, 5:365-368.
- Chennakesava R. Alavala (2009): *Finite Element Methods: Basic Concepts and Applications*, PHI Learning Pvt. Ltd, New Delhi.
- Hojo, H., Toyoshima, W., Tamura, M., and Kawamura, N. (1974): Short- and long- term strength characteristics of particulate-filled cast epoxy resin, *Poly. Eng. Sci.*, 14:604-609.
- Ishai, O., Cohen I.J. (1967): Elastic properties of filled and porous epoxy composites, *Int. J. Mech. Sci.*, 9:539-546.
- Kamat, S.V., Hirth, J.P., and Mehrabian, R. (1989): Mechanical properties of particulate-reinforced aluminum-matrix composites, *Acta Metall.*, 37:2395-2402.
- Pestes, R. H., Kamat, S.V., and Hirth, J.P. (1994): Fracture toughness of Al-4%Mg/Al₂O₃ composites, *Mat. Sci.Eng.*189A:9-14.
- Punkanszky, B., Turcsanyi, B., and Tudos, F. (1988): Effect of interfacial interaction on the tensile yield stress of polymer composites, In: H. Ishida, editor, *Interfaces in polymer, ceramic and metal matrix composites*, Amsterdam: Elsevier, 467-77.
- Reddy, A. C. (2009): Mechanical properties and fracture behavior of 7020/SiCp Metal Matrix Composites Fabricated by Low Pressure Die Casting Process, *J. Manuf. Technol. Res.*, 1:273-286.
- Reddy, A. C. Essa, Z. (2010): Tensile behavior of 6063/Al₂O₃ particulate metal matrix composites fabricated by investment casting process, *Int. J. Applied Eng. Res.*, 1:542-552.
- Redsten, A. M., Klier, E. M., Brown, A. M., and Dunand, D. C.(1995): Mechanical properties and microstructure of cast oxide-dispersion-strengthened aluminum, *Mat. Sci. Eng.*, 201A:88-102.
- Rohatgi, P.K., Asthana, R., and Das, S. (1986): Solidification, Structures and Properties of Cast Metal-Ceramic Particle Composites. *Int. Mater. Rev.*, 31:115-139.
- Srivatsan, T.S. (1996): Microstructure, tensile properties and fracture behavior of Al₂O₃ particulate-reinforced aluminum alloy metal matrix composites, *J.Mat. Sci.*, 31:1375-1388.